Helmholtz-Zentrum Dresden-Rossendorf (HZDR)

HELMHOLTZ ZENTRUM
DRESDEN ROSSENDORF

Zwitterionic Modification of Ultra-Small Iron Oxide Nanoparticles for Reduced Protein Corona Formation

Pombo-Garcia, K.; Rühl, C.; Lam, R.; Ang, C.-S.; Scammells, P. J.; Comba, P.; Spiccia, L.; Graham, B.; Joshi, T.; Stephan, H.;

Originally published:

March 2017

ChemPlusChem 82(2017), 638-646

DOI: https://doi.org/10.1002/cplu.201700052

Perma-Link to Publication Repository of HZDR:

https://www.hzdr.de/publications/Publ-25079

Release of the secondary publication
on the basis of the German Copyright Law § 38 Section 4.

Zwitterionic Modification of Ultra-Small Iron Oxide Nanoparticles for Reduced Protein Corona Formation

Karina Pombo-García,[a]^ Carmen Rühl,[b]^ Raymond Lam,[c] José A. Barreto,[d] Ching-Seng Ang,[e] Peter J. Scammells,[c] Peter Comba,[b] Leone Spiccia,[d] Bim Graham,*[c] Tanmaya Joshi,*[a] and Holger Stephan*[a]

Dedicated to the memory of our friend, colleague and mentor, Prof. Leone Spiccia, who passed away on the 18th December 2016

Abstract: Polyacrylic acid-coated ultra-small super-paramagnetic iron oxide nanoparticles have been surface-modified with low-molecular weight sulfobetaines or *N,N*-diethylaminopropylamine in order to generate nanoparticles with zwitterionic character (ZW-NPs). The ZW-NPs proved highly resistant to serum protein corona formation *in vitro*, as revealed by AFM, SDS-PAGE and proteomics analysis, and exhibited low cytotoxicity towards A431 and HEK293 cells. The presence of unreacted carboxylic acid groups enabled additional functionalization with fluorescent (Cy5) and radioactive (^{64}Cu-dmptacn) moieties. Overall, the ZW-NPs represent promising platforms for the development of new multi-modal diagnostic/therapeutic agents possessing "stealth" properties.

Introduction

The success of ultra-small super-paramagnetic iron oxide nanoparticles (USPIONs) in *in vivo* biomedical applications, e.g., magnetic resonance imaging (MRI), relies on chemical modifications that lead to controlled biodistribution, reduced toxicity and extended circulation times within the bloodstream.[1-8] Appropriate surface modification of USPIONs so as to fulfil these pharmacokinetic requirements presents a key challenge. It is particularly important that USPIONs are able to resist extensive non-specific adsorption of proteins ("protein corona" formation) and opsonization, so as to avoid rapid scavenging by the mononuclear phagocyte system (MPS).[1-2, 6-10] One way to achieve this is through the introduction of zwitterionic (ZW) species onto the nanoparticle (NP) surface.[1-2, 6, 10-26] Zwitterionic surfaces confer similar anti-fouling properties to poly(ethylene glycol) (PEG) coatings, but without adding substantially to the hydrodynamic size of the coated NPs. ZW-NPs are also less prone to aggregation under high ionic strength conditions.[1, 17, 21, 24-31]

Recently, we reported a detailed *in vitro* investigation of the "stealth" properties of USPIONs coated with poly(maleic anhydride-alt-1-decene) substituted with 3-(dimethylamino)propylamine (PMAL), an amphiphilic zwitterionic polymer.[15, 32] The PMAL-USPIONs proved superior to USPIONs coated with octylamine-modified polyacrylic acid, a negatively charged polymer, in terms of their ability to resist protein corona formation.[15] Encouraging results from this study, along with a continued interest in developing NP-based multi-modal imaging agents for *in vivo* use, have now led us to explore the effect of zwitterionic modifications on the properties of polyacrylic acid-coated USPIONs (PAA-USPIONs). Herein, we present the results of a study examining the serum protein adsorption characteristics, cellular uptake and cytotoxicity of PAA-USPIONs functionalised with three low-molecular weight compounds that impart zwitterionic character to the NP surface. Given that previous studies have shown that the interactions of NPs with proteins and cells are nanomaterial-specific and dictate their ultimate metabolic fate,[10, 14, 16, 21-23, 29, 33-37] examination of such interactions represents an important first step in the development of new nanomaterials intended for *in vivo* use.

Results and Discussion

Synthesis and physicochemical characterization of zwitterionic nanoparticles

Water-soluble, PAA-USPIONs were prepared via the co-precipitation method described by Rosseinsky and

[a] Dr. K. Pombo-Garcia, Dr. T. Joshi, Dr. H. Stephan
Institute of Radiopharmaceutical Cancer Research
Helmholtz-Zentrum Dresden-Rossendorf
D 01328 Dresden, Germany
Email: t.joshi@hzdr.de; h.stephan@hzdr.de

[b] MSc. C. Rühl, Prof. P. Comba
Heidelberg University,
Institute of Inorganic Chemistry and Interdisciplinary Centre for Scientific Computing
Im Neuenheimer Feld 270,
69120 Heidelberg, Germany

[c] R. Lam, Prof. P. J. Scammells, Assoc. Prof. B. Graham
Monash Insitute of Pharmaceutical Sciences
Monash University
Parkville, VIC 3052, Australia
Email: bim.graham@monash.edu

[d] Dr. J. A. Barreto, Prof. L. Spiccia
School of Chemistry
Monash University
Clayton, VIC 3800, Australia

[e] Dr. C.-S. Ang
BIO21 Molecular Science and Biotechnology Institute
The University of Melbourne
Melbourne, VIC 3010, Australia

[^] *These authors contributed equally to this work.*

Supporting information for this article is given via a link at the end of the document.

WILEY-VCH

co-workers.[38] To reduce the negative surface charge and impart zwitterionic character to the NPs, one of three compounds (**L1**, **L2** or **L3**) was covalently attached to their surface employing EDC/sulfo-NHS coupling conditions (Figure 1).[2] **L1** and **L2** are sulfobetaines, a class of compounds that has been widely employed in the development of zwitterionic coatings,[11, 19, 39-41] while **L3** (*N,N*-diethylaminopropylamine) has been previously employed by Xiao *et al.* to generate NPs with long *in vivo* circulation times.[21] The new zwitterionic USPIONs, **ZW-L1**, **ZW-L2** and **ZW-L3**, were purified by size-exclusion chromatography (SEC).

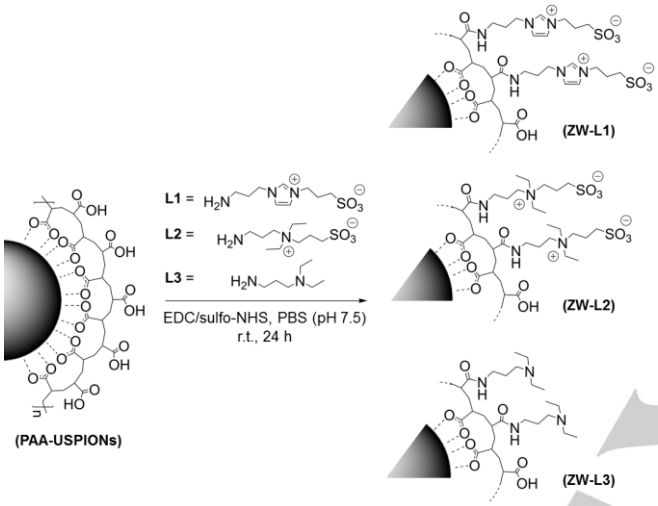

Figure 1. Surface modification of PAA-USPIONs with **L1**, **L2** and **L3** to generate ZW-NPs, **ZW-L1**, **ZW-L2**, and **ZW-L3**, respectively.

Transmission electron microscopic (TEM) analysis (Figure 2A) revealed that the USPIONs remained unaggregated after surface modification, retaining a reasonably uniform iron oxide core diameter of 5–6 nm, while dynamic light scattering (DLS) measurements indicated a small increase in the hydrodynamic diameter (HD) (11.7 ± 1.3 nm, 12.8 ± 2.0 nm and 14.0 ± 2.3 nm for **ZW-L1**, **ZW-L2** and **ZW-L3**, respectively, *versus* 8.3 ± 0.3 nm for PAA-USPIONs) (Figure 2B). The overall negative surface charge of the NPs decreased (zeta potential, ζ = -21.7 ± 0.4 mV, -15.7 ± 2 .1 mV, -16.0 ± 3.1 mV for **ZW-L1**, **ZW-L2** and **ZW-L3**, respectively, *versus* -42.3 ± 1.5 mV for PAA-USPIONs) (Figure 2C), which can be ascribed to the expected reduction in the number of surface carboxylate groups after attachment of compounds **L1–L3**.

Elemental microanalyses confirmed the presence of nitrogen and sulfur within **ZW-L1**, **ZW-L2**, and the presence of nitrogen within **ZW-L3**, providing further evidence for successful attachment of **L1–L3** to the surface of the USPIONs. FTIR spectra showed bands attributable to amide and carboxylic acid functionalities within **ZW-L1**, **ZW-L2** and **ZW-L3**, as well as the sulfonate groups in **ZW-L1** and **ZW-L2** (Figure 2D). Bands within the region 1700–1400 cm^{-1} are related to the $C{=}O_{stretch}$, $C\text{-}O\text{-}H_{bend}$ and $C\text{-}O_{stretch}$ vibrations of the carboxylic acid groups.[2] In accordance with the expectation that successful coupling would decrease the amount of free carboxylic acid groups in ZW-NPs, the relative intensities of these bands are lower in the spectra of **ZW-L1**, **ZW-L2** and **ZW-L3**. Prominent bands in the region of 1100–850 cm^{-1} correspond to $C\text{-}H_{bend}$, $SO_{2\ stretch}$ and $S\text{-}O_{stretch}$ vibrations. Amide I and II bands are visible between 1500 and 1600 cm^{-1}, and a $Fe\text{-}O_{stretch}$ vibration band at 580 cm^{-1}.[2]

The ZW-NPs displayed good colloidal stability under physiological conditions, with no signs of aggregation in response to pH changes in the range of 6–10 after 24 h incubation. Figure 2E shows representative photographs of aqueous dispersions of **ZW-L1** at a range of different pHs, highlighting their stability.

Analysis of serum protein-nanoparticle interactions

The ability of the ZW-NPs to resist serum protein adsorption was evaluated using a combination of atomic force microscopy (AFM), sodium dodecyl sulfate polyacrylamide gel electrophoresis (SDS-PAGE) and proteomics analysis.

Figures 3A,B show representative AFM images of **ZW-L1** after 30 min of exposure to 80% human serum (HS). The NPs remained well-dispersed and did not increase beyond *ca.* 12 nm in diameter. In contrast, PAA-USPIONs formed large aggregates (*ca.* 100 nm diameter) upon exposure to HS (Figures 3C, D).

The absence of significant protein corona formation for **ZW-L1, ZW-L2** and **ZW-L3** was further confirmed through SDS-PAGE analysis of adsorbed serum proteins (removed by denaturation and heating to 95°C with 2x Laemmli sample buffer containing 2-mercaptoethanol). As shown in Figure 4A, only very faint protein bands were observed compared to those found for PAA-USPIONs exposed to 80% HS.

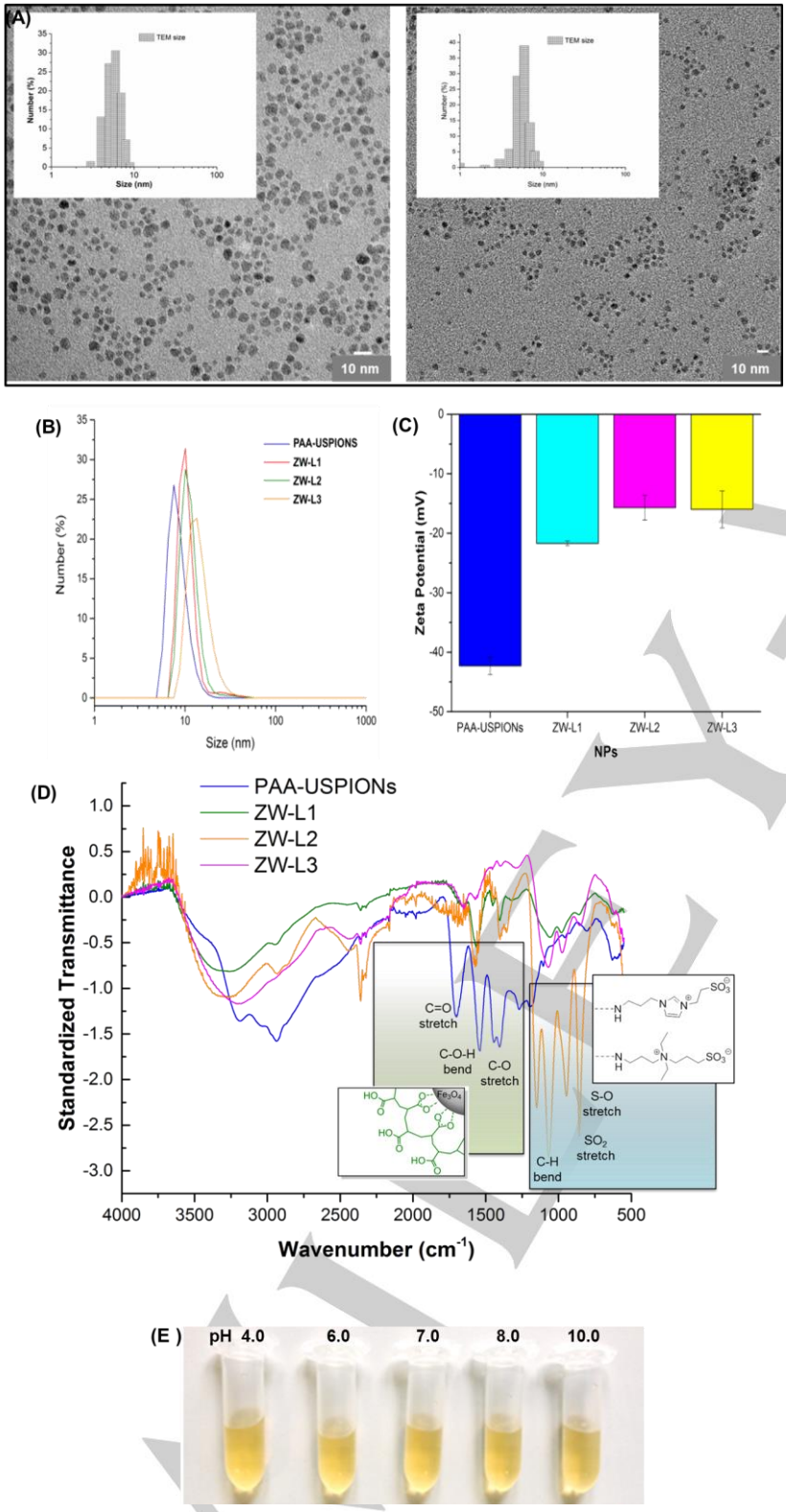

Figure 2. Physicochemical characterization of NP samples. (A) TEM micrographs showing well-dispersed PAA-USPIONs (left) and **ZW-L1** (right) with a uniform core diameter of 5–6 nm. Inserts are size distributions derived from the analysis of 200 NPs. (B) HD of PAA-USPIONs (8.3 ± 0.3 nm), **ZW-L1** (11.7 ± 1.3 nm), **ZW-L2** (12.8 ± 2.0 nm) and **ZW-L3** (14.0 ± 2.3 nm), as measured by DLS. (C) Zeta potential of PAA-USPIONs (-42.3 ± 1.5 mV), **ZW-L1** (-21.7 ± 0.4 mV), **ZW-L2** (-15.7 ± 2.1 mV) and **ZW-L3** (-16.0 ± 3.1 mV) (50 mM, pH 7.5). (D) IR spectra of NPs. (E) Photographs of aqueous dispersions of **ZW-L1** at different pHs (4–10).

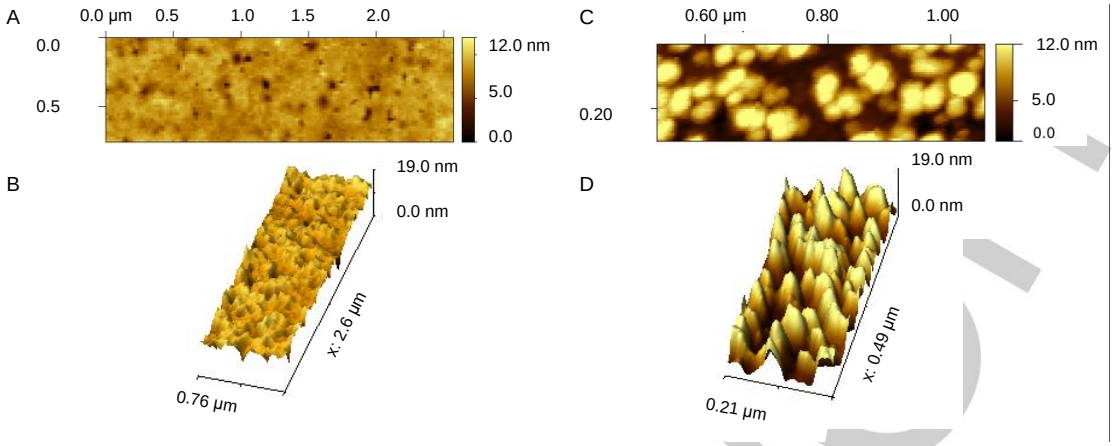

Figure 3. AFM micrographs of (A, B) **ZW-L1** and (C, D) PAA-USPIONs after incubation with 80% HS for 30 min. (A) and (C) are height images (scan size = 2.6 x 0.76 µm), while (B) and (D) are 3D images (scan size = 0.21 x 0.49 µm).

The identity of the NP-binding proteins was established using mass spectrometry-based proteomics techniques. At the same time, relative quantification of the amounts of individual proteins within the coronas of the serum-exposed ZW-NPs *versus* that of the PAA-USPIONs was carried out using isotope dimethyl labeling.[15, 42-43] This involved detachment of the adsorbed proteins using a denaturant containing 8 M urea, followed by reduction, digestion with trypsin, and labeling with non-deuterated ("light") formaldehyde in the case of the PAA-USPIONs and deuterated ("heavy") formaldehyde in the case of the ZW-NPs. The labeled tryptic digests were then mixed in equal amounts for each PAA-USPIONs/ZW-NPs combination and analyzed by LC-MS/MS in order to determine the identity and relative quantity of adsorbed proteins.[15, 43] Only two, nine and ten serum proteins were identified with a high degree of confidence in the coronas of **ZW-L1**, **ZW-L2** and **ZW-L3**, respectively (Figure 4B). One of these was common to all three protein coronas, and a further seven to the coronas of **ZW-L2** and **ZW-L3**. The majority of the identified proteins were vastly enriched in the corona of the PAA-USPIONs relative to those of the ZW-NPs (Tables S1–S3).

Collectively, these data suggest that **L1**, the imidazolium-containing sulfobetaine derivative, is most effective in reducing protein corona formation, and provide further evidence of the ability of zwitterioinic surfaces in general to limit protein corona formation and enhance NP stability within biological fluids.[3-4, 8, 36, 44-45] Reduced protein adsorption in serum has previously been observed for Au NPs featuring zwitterionic sulfobetaine groups,[11] and we have recently reported similar behaviour for other zwitterionic polymer-coated USPIONs.[15]

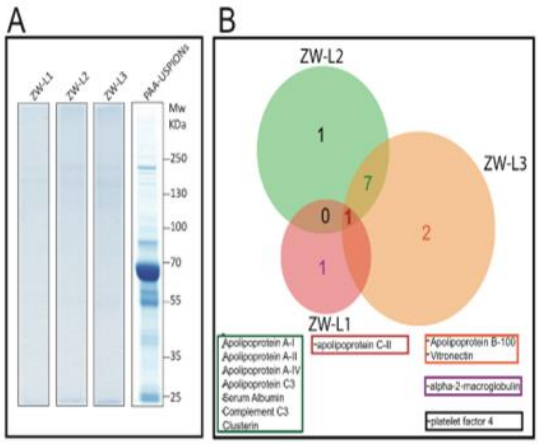

Figure 4. Analysis of HS proteins adsorbed by ZW-NPs and PAA-USPIONs. (A) Coomassie-stained 12% SDS-polyacrylamide gel of adsorbed proteins. (B) Venn diagram of all proteins identified by proteomic analysis within the protein coronas of the HS-exposed ZW-NPs (refer to Tables S1–S3 for detailed list of identified proteins).

Cellular uptake and cytotoxicity of nanoparticles

Next, we investigated the cellular uptake properties of the ZW-NPs. A431 cancer cells were exposed to ZW-NPs in serum-free media as well as cell media supplemented with 10% and 100% fetal bovine serum (FBS) for 24 h, followed by ICP-MS analysis to quantify the concentration of Fe arising from the magnetite core of the NPs (prior experiments performed in the absence of NPs confirmed that the cells were able to grow under all conditions examined). A control without NPs was used to quantify the cellular iron concentration. As shown in Figure 5, very low cellular uptake was observed for all three of the ZW-NPs, with values ranging from 1 to 10 picograms Fe per cell. Further, the uptake decreased with increasing serum concentration, i.e., very little uptake was detected in 100% FBS. In the presence of an excess of proteins, NPs that do not possess a protein corona have a lower probability of interacting with the cellular membrane, thus slowing down their endocytic uptake by the cell, which is concordant with our findings for other NPs.[15, 32] A noteworthy observation is the *ca.* 5-fold greater uptake of **ZW-L3** *versus* **ZW-L1** and **ZW-L2**, which is in accordance with the differing degrees of protein corona formation for the ZW-NPs.

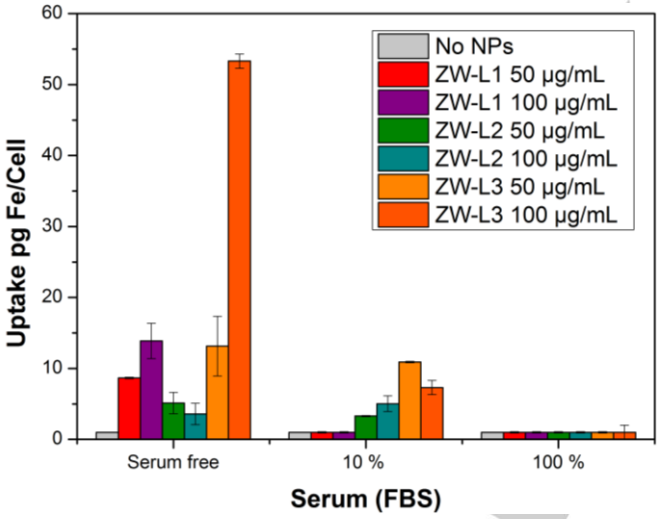

Figure 5. Degree of uptake of ZW-NPs into A431 cells in the absence or presence of 10% or 100% FBS. Cells were incubated with 50 or 100 µg/mL of ZW-NPs for 24 h before digestion.

To assess cell viability following exposure to the ZW-NPs, the metabolic activities of both cancerous (A431) and non-cancerous cells (HEK293) cells were measured using an MTS cell proliferation assay (Figures 6A,B). In addition, membrane integrity as a measure of viability and necrosis was assessed by monitoring the NP-induced leakage of active lactate dehydrogenase (LDH) into the cell culture media (Figures 6C,D). The ZW-NPs showed low and comparable cytotoxic responses up to their highest dosed concentrations (100 µg/mL), indicating no major damage to the mitochondria (MTS assay) or lysis of the cell membrane upon incubation (LDH assay).

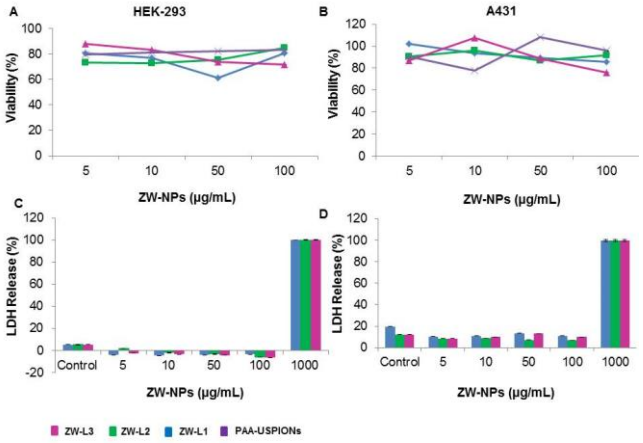

Figure 6. Nanotoxicity assessment of ZW-NPs and PAA-USPIONs. (A, B) Viability of A431 and HEK293 cells measured after 24 h exposure to increasing concentrations of NPs, expressed as a percentage with respect to the negative control (cells without NPs). (C, D) LDH release from A431 and HEK293 cells measured after 24 h exposure to increasing concentrations of NPs. LDH release was measured in triplicate. Cells were incubated with supplied lysis buffer to obtain maximum LDH release (positive control).

Generation of bimodal imaging agents

The availability of unreacted carboxylate functionalities prompted us to investigate the possibility of conjugating additional moieties to the surface of the ZW-NPs, thereby providing a facile route to access bi/multimodal imaging agent designs. In the first instance, covalent attachment of a near-infrared fluorescent dye (Cy5) to **ZW-L1** was investigated, with the aim of instilling optical imaging (OI) capability. Employing conventional EDC/sulfo-NHS-mediated coupling conditions,[15, 32] an amine-bearing derivative of Cy5 was successfully linked to the NPs (Figure 7), as verified by UV-Vis absorption and photoluminescence spectroscopic measurements (Figure 8), performed following SEC purification to remove low-molecular weight material. The spectra displayed the characteristics absorption and emission bands of Cy5, with the λ_{max} values (*ca.* 650 and 655 nm, respectively) slightly red-shifted relative to those of "free" Cy5, as already reported for other dye-NP interfaces.[46] A fluorescence quantum yield of 0.18 was determined, which is about two-thirds that of free Cy5,[47] presumably due to self-quenching effects or quenching by the iron oxide core of the NPs.

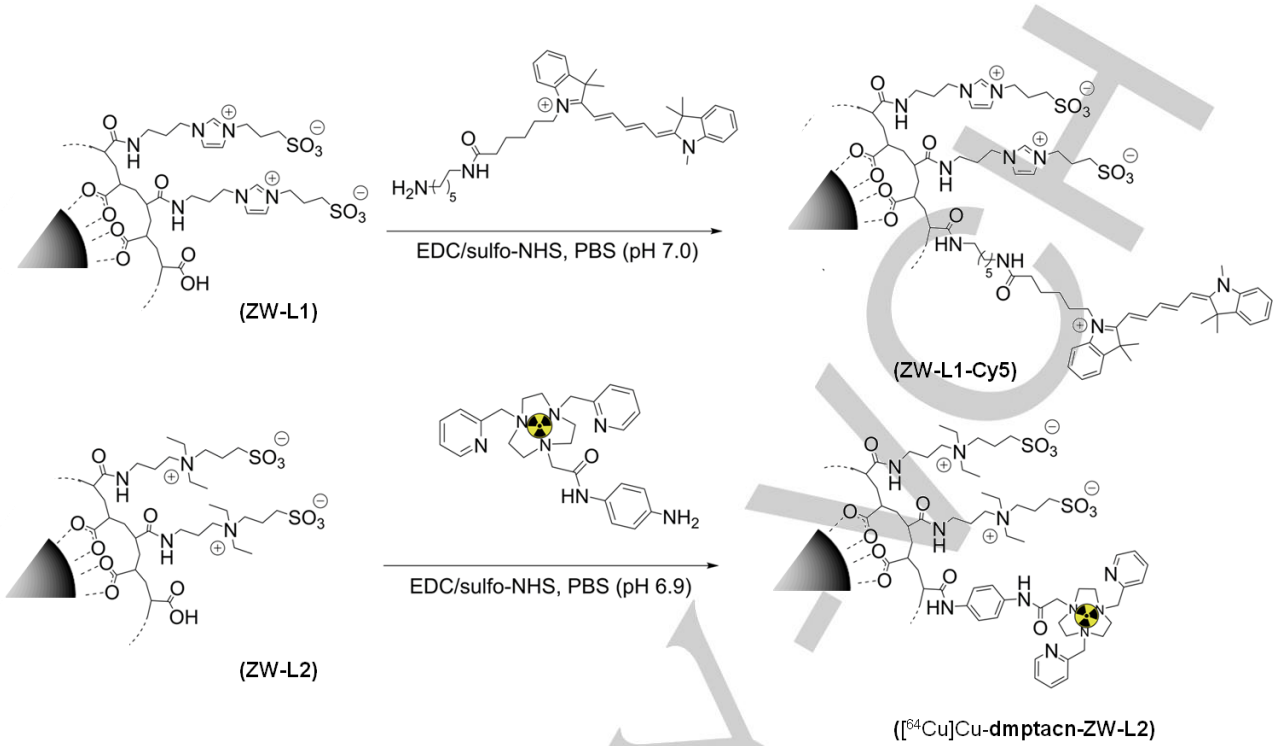

Figure 7. Conjugation of a near-infrared fluorophore (Cy5) and a radiochelate ([^{64}Cu]Cu-dmptacn) to ZW-NPs to generate potential bimodal MRI/OI and MRI/PET imaging agents.

To generate a potential design for dual imaging by MRI and positron emission tomography (PET), a preformed ^{64}Cu complex ([^{64}Cu]Cu-dmptacn)[32] was coupled to **ZW-L2**, also employing EDC/sulfo-NHS-mediated coupling (Figure 7). Radio-SEC was used to remove unreacted complex and confirm successful radiolabeling of the NPs (Figure 9A). The ^{64}Cu-labeled-NPs were found to be resistant to metal ion leakage when challenged with EDTA for a 24 h period, as indicated by radio-TLC analysis (Figure 9B). It should be noted that a post-labeling strategy was also attempted, in which the dmptacn chelator was first attached to the NPs and then complexation of $^{64}Cu^{2+}$ ions attempted. However, the results obtained were not promising, with a very low radiochemical yield obtained.

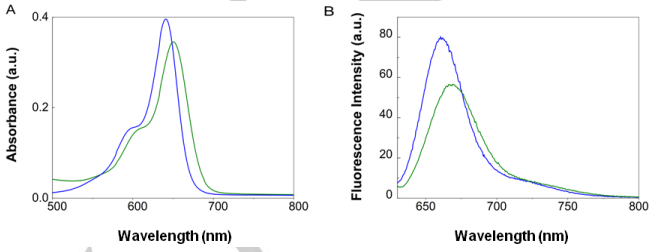

Figure 8. (A) Electronic absorbance and (B) emission spectra of Cy5-functionalized **ZW-L1** (green) and free Cy5 (blue).

Overall, these results clearly demonstrate that tethering additional groups to the ZW-NPs is feasible, despite them having a reduced number of carboxylate functionalities on their surface after zwitterionic modification.

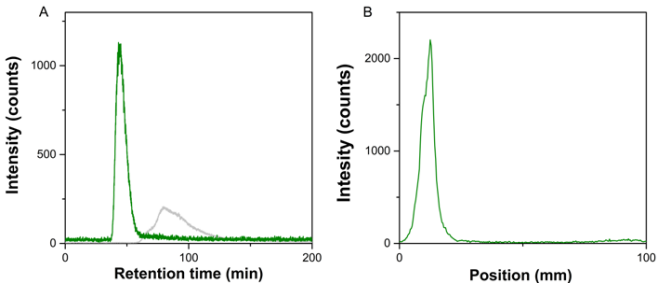

Figure 9. Analysis of [^{64}Cu]Cu-dmptacn-labeled **ZW-L2**. (A) Radio-SEC of [^{64}Cu]Cu-dmptacn-labeled **ZW-L2** (green) and [^{64}Cu]Cu-dmptacn (gray) (B) Radio-TLC of EDTA-challenged [^{64}Cu]Cu-dmptacn-labeled **ZW-L2** (R_f = 0 *versus* 0.8 for [^{64}Cu]Cu-EDTA) recorded using a neutral Al_2O_3 stationary phase and a 1:1 (*v/v*) 2 M NH_4OAc/MeOH mobile phase.

Conclusion

In summary, the studies reported herein have successfully demonstrated that modifying the surface of PAA-USPIONs with

sulfobetaines or *N,N*-diethylaminopropylamine is an effective strategy for limiting protein corona formation. AFM, SDS-PAGE and proteomics analysis all showed that adsorption of serum proteins was greatly reduced by imparting a degree of zwitterionic character to the NP surface. The ZW-NPs exhibit minimal cytotoxicity (A431 cells) and only very low levels of cellular uptake (A431 and HEK293 cells). We have shown that a fluorophore and a radiochelate can be readily coupled to the NPs. Collectively, these results indicate that the ZW-NPs provide an attractive foundation for the development of "stealth" multimodal imaging and theranostic agents. Our future research efforts will focus on exploring the *in vivo* behavior of the NPs, as well as the development of more sophisticated designs featuring a combination of bifunctional chelators, dye molecules, active targeting agents (peptides, antibodies, etc.) and/or therapeutic agents attached to the NP surface.

Experimental Section

Materials

All chemicals and solvents were purchased from reputable commercial suppliers and used as received without further purification. Compound **L2** and the [^{64}Cu]Cu-dmptacn radiochelate were synthesized by adapting the literature procedures described by Kim *et al.*[48] and Pombo-Garcia *et al.*,[32] respectively**.** Ultrapure water with resistivity 18 MΩ cm was obtained from an inline Millipore RiOs/Origin System (Millipore Corporation, USA).

Instrumentation and methods

^{1}H and ^{13}C nuclear magnetic resonance (NMR) spectra were recorded using an Avance III Nanobay 400 MHz Bruker spectrometer coupled to the BACS 60 automatic sample changer at 400.13 MHz and 100.61 MHz, respectively. Data acquisition and processing was managed using Topspin software package version 3. Additional processing was handled with MestReNova software (PC). Chemical shifts (δ) were measured in parts per million, referenced to an internal standard of residual solvent.[49] Spectroscopic data are given using the following abbreviations: s, singlet; d, doublet; dd, doublet of doublets; dt, doublet of triplets; t, triplet; app p, apparent pentet; m, multiplet; *J*, coupling constant. Mass spectrometry (MS) was performed using an Agilent 6100 Series Single Quad LC-MS coupled to an Agilent 1200 Series HPLC with the following mass spectrometer conditions: multimode-ESI mode, 300°C drying gas temperature, 200°C vaporizing temperature, capillary voltage of 2000 V (positive), capillary voltage of 4000 V (negative), scan range between 100–1000 *m/z* with an 0.1 sec step size and a 10 min acquisition time. Absorbance spectra were recorded on a Varian Cary 50 Bio UV-Vis spectrophotometer. Fluorescence emission spectra were acquired using a Varian Cary Eclipse fluorescence spectrophotometer.

Synthesis of L1

N-(3-Phthalimidopropyl)imidazole (**1**). A mixture of imidazole (2.96 g, 44.8 mmol), *N*-(3-bromopropyl)phthalimide (4.00 g, 14.9 mmol) and K_2CO_3 (2.06 g, 14.9 mmol) in MeCN (30 mL) was refluxed for 17 h. The reaction mixture was then cooled to room temperature (r.t.) and filtered. The filtrate was evaporated and the resulting residue purified by flash chromatography (9:1 (*v/v*) $CHCl_3$/MeOH on silica) to obtain **1** as an off-white solid (1.81 g, 48%). ^{1}H NMR (400 MHz, C*D*Cl$_3$): *δ* 7.85–7.78 (m, 2H), 7.75–7.66 (m, 2H), 7.58 (s, 1H), 7.02 (s, 1H), 6.98 (t, *J* = 1.2 Hz, 1H), 4.00 (t, *J* = 7.0 Hz, 2H), 3.71 (t, *J* = 6.6 Hz, 2H), 3.44 (s, 1H), 2.17 (app p, *J* = 6.8 Hz, 2H) ppm. ^{13}C NMR (101 MHz, C*D*Cl$_3$): *δ* 168.4, 137.2, 134.3, 131.9, 129.4, 123.5, 118.9, 50.5, 44.6, 35.2, 30.2 ppm. MS: *m/z* 256.2 $[M+H]^+$.

1-(3-Phthalimidopropyl)-3-(3-sulfonatopropyl)imidazolium (**2**). Compound **1** (1.79 g, 7.03 mmol) and 1,3-propanesultone (0.944 g, 7.73 mmol) were added to dry MeCN (40 mL) and the mixture was refluxed for 3 h. After cooling the reaction mixture to r.t., the formed precipitate was collected by filtration, washed with $CHCl_3$ and air-dried to obtain **2** as a white solid (2.26 g, 85%). ^{1}H NMR (400 MHz, DMSO-d_6): δ 9.19–9.11 (m, 1H), 7.93–7.81 (m, 4H), 7.79 (dd, *J* = 3.3, 1.6 Hz, 2H), 4.29 (t, *J* = 6.9 Hz, 2H), 4.22 (t, *J* = 7.3 Hz, 2H), 3.61 (t, *J* = 6.3 Hz, 2H), 2.42 (t, *J* = 7.1 Hz, 2H), 2.17 (dt, *J* = 13.5, 6.8 Hz, 2H), 2.13–2.04 (m, 2H) ppm. ^{13}C NMR (101 MHz, DMSO-d_6): δ 168.1, 136.4, 134.4, 131.9, 123.1, 122.5, 122.3, 47.9, 47.3, 46.6, 34.4, 28.5, 26.2 ppm. MS: *m/z* 378.2 $[M+H]^+$.

1-(3-Aminopropyl)-3-(3-sulfonatopropyl)imidazolium trifluoroacetate (**L1·TFA**). To a suspension of compound **2** (2.24 g, 5.94 mmol) in MeOH (50 mL) was added N_2H_4•H_2O (2.88 mL) and the mixture refluxed for 2 h, during which time a white precipitate formed. The reaction mixture was cooled to r.t. and filtered. The filtrate was concentrated under reduced pressure and the resulting crude residue purified by reverse-phase chromatography (0.1% TFA in water on C18 silica) to obtain **L1** as a yellow oil, isolated as a TFA salt (1.86 g, 86%). ^{1}H NMR (400 MHz, DMSO-d_6): *δ* 9.20 (s, 1H), 7.81 (dt, *J* = 20.1, 1.7 Hz, 2H), 4.29 (dt, *J* = 16.8, 6.9 Hz, 4H), 2.85–2.76 (m, 2H), 2.46 (t, *J* = 7.2 Hz, 2H), 2.17–2.03 (m, 4H) ppm. ^{13}C NMR (101 MHz, DMSO-d_6): *δ* 136.5, 122.8, 122.4, 47.9, 47.4, 46.0, 35.9, 27.7, 26.0 ppm. MS: *m/z* 248.2 $[M+H]^+$.

General procedure for synthesis of zwitterionic nanoparticles

Polyacrylic acid-coated USPIONs were prepared *via* the co-precipitation method reported by Li *et al*.[38] For the coupling reactions, EDC (5.2 mg, 27 µmol) and sulfo-NHS (5.8 mg, 27 µmol) in 50 mM phosphate buffer (pH 6.0) were added to the PAA-USPIONs (5 mg). A solution (0.5 mL) of **L1**, **L2** or **L3** (13.5 *µ*mol) or diethylaminopropylamine (DEAPA) in 300 mM phosphate buffer (pH 7.5) was then added to the activated PAA-USPIONs. The pH of the mixture was adjusted to 7.5 by addition of 3 mL of 300 mM phosphate buffer (pH 7.5), and the reaction solution stirred for 24 h at 37°C. After purification by size-exclusion chromatography (Sephadex G-25 fine, eluting with 100 mM phosphate buffer, pH 7.5) and subsequent filtration through a 0.2 µm membrane, **ZW-L1**, **ZW-L2**, **ZW-L3** were stored at 4°C until further required. The concentrations of Fe were measured by inductively-coupled plasma mass spectrometry (ICP-MS, ELAN 9000, Perkin Elmer) and used to calculate the final concentrations of the NPs. The measurements were performed with an internal rhodium standard and a standard curve constructed using ICP standard solutions, e.g., Fe in 0.5 M HNO_3 (Bernd Kraft GmbH).

Cy5-labeled **ZW-L1** and [^{64}Cu]Cu-dmptacn-labeled **ZW-L2** were prepared and characterized employing previously described methods.[15, 32]

Particle characterization techniques

TEM images of the NPs were recorded on a FEI Tecnai G 2 T20 transmission electron microscope with an accelerating voltage of 200 kV and a lanthanum hexaboride (LaB6) thermal emitter. Images were taken with a Gatan Orius SC camera and edited using the Gatan "Digital Micrograph" program. Samples were prepared by dipping an ultrathin carbon copper grid in a diluted solution of NPs in MilliQ water. The hydrodynamic diameter (HD) of the NPs in the presence of 10 mM NaCl

was determined by dynamic light scattering (DLS), and zeta potentials were determined by Laser Doppler velocimetry (Zetasizer Nano ZS Malvern Instruments, UK). Infrared spectra (4000–550 cm^{-1}) were recorded on solid samples of the NPs with a Thermo Fisher Scientific (Waltham, Massachusetts, United States) FTIR spectrometer using the ATR technique. Elemental analyses were performed on a EuroEA 3000 instrument from EuroVector (Milan, Italy).

Atomic force microscopy

AFM was performed using a Multimode 8 scanning probe microscope (Bruker) and PP-NCLR cantilevers from Nanosensors (nominal force constant 48 N m^{-1}, tip radius < 10 nm). Images were processed using Gwyddion open source software. Samples were prepared by adding 20 µL of a 30 µg/mL stock of NPs, previously incubated for 30 min at 37°C with water or human serum (HS), to a freshly-cleaved mica surface and air-drying before imaging.

Protein isolation from nanoparticles and sodium dodecyl sulfate polyacrylamide gel electrophoresis

NP samples were incubated in HS at different dilutions for 30 min at 37°C. After incubation, serum-NP mixtures were centrifuged for 4 h at 20,000 x g. In each case, the supernatant was carefully removed and the pellet washed four times with PBS (1 mL) by suspension in solution followed by pelleting and removal of supernatant (a serum-only sample showed no sedimentation of free proteins under such conditions). Proteins were eluted from the NP surfaces by adding 2x Laemmli Sample Buffer (Bio-Rad) with 2-mercaptoethanol to the final pellets and subsequent incubation at 95°C for 5 min. For SDS-PAGE, recovered proteins in sample buffer (20 µL) were separated on a 4–12% SDS-PAGE gel (NuPAGE®, Invitrogen). PageRuler™ Plus Prestained Protein Ladder (Thermo Scientific) was used as marker and 1x MOPS (Invitrogen) as running buffer. Gels were run at 120 V for 1.3 h and Coomassie staining (InstantBlue™, Expedeon) was performed to visualize the bands.

Identification and relative quantification of proteins through dimethyl labeling

For the relative quantitative proteomics analysis, NPs were incubated in triplicate with 50% HS for 30 min at 37°C. Washing of the NPs was performed in the same way as described for the SDS-PAGE. Detachment of the bound proteins from the corona of the NPs was achieved using 8 M urea in 25 mM TEAB. The proteins were then reduced, alkylated and digested using sequencing grade trypsin, and labeled with formaldehyde (CH_2O for PAA-USPIONs and CD_2O for either **ZW-L1**, **ZW-L2** or **ZW-L3**) following a previous protocol published by Boersema *et al*.[43] Finally, both labeled samples (for each single experiment) were mixed and analyzed by LC-MS/MS as described below.

Mass spectrometry and data analysis

Tryptic digests were analyzed by LC-MS/MS using a LTQ Orbitrap Elite (Thermo Scientific) with a nanoelectrospray interface coupled to an Ultimate 300 RSLC nanosystem (Dionex) The nanoLC system was equipped with an Acclaim Prepmap Nanotrap column (Dionex C18, 100 Å, 75 µm x 2 cm) and an Acclaim Pepmap analytical column (Dionex C18, 2 µm, 100 Å, 75 µm x 15 cm). An aliquot of the digestion mix (2 µL) was loaded onto the trap column with an isocratic flow of 4 µL/min of 3% CH_3CN containing 0.1% formic acid for 5 min before the enrichment column was switched in-line with the analytical column. The eluents used for the liquid chromatography were 0.1% (*v/v*) formic acid (solvent A) and 100% CH_3CN/0.1% formic acid (*v/v*) (solvent B). The following gradient was used: 3% to 12% for 1 min, 12% to 35% B for 20 min, 35% to 80% B for 2 min, and then constant 80% B for 2 min, followed by equilibration at 3% B for 7 min before the next sample injection. The LTQ Orbitrap Elite mass spectrometer was operated in the data-dependent mode with a nano ESI spray voltage of +2.0 kV, a capillary temperature of 250°C, and an S-lens RF value of 60%. Spectra were acquired first in positive mode with full scan, scanning from *m/z* 300 to 1650 in the FT mode at 240000 resolution followed by collision-induced dissociation in the linear ion trap with the ten most intense peptide ions with charge states ≥ 2 isolated and fragmented using a normalized collision energy of 35 and an activation Q of 0.25.

Data analysis was performed using Proteome Discoverer (Thermo Scientific, version 1.4) with Mascot search engine (Matrix Science version 2.4) against the Uniprot database for the human genome. The search parameters included a precursor mass tolerance of 20 ppm, fragment mass tolerance of 0.6 Da, carbamidomethyl of cysteine as fixed modification, and dimethyl labeling (CH_2O + 28.031 Da; CD_2O + 32.056 Da) at the peptide N-terminus and lysine set as variable modifications. Trypsin with no missed cleavages was used as the cleavage enzyme. Search results were set to a maximum of 1% false discovery rate (FDR) and at least two unique peptides required for positive identification.[23] Quantification of the dimethyl-labeled peptides was conducted using the Quant node on Proteome Discoverer, which works by extracting and comparing the area of the light and heavy labelled peptides. To add further confidence, proteins were filtered against the human plasma proteome database.[50]

Cell culture

Cell culture flasks, dishes and plates (CELLSTAR®) were supplied by Greiner Bio-One GmbH. The epidermoid human cancer cell line A431 (ATCC® number: CRL-1555) and the human embryonic kidney cell line HEK293 (DMSZ number: ACC 305) were cultured as previously reported.[15, 51] All cell lines were confirmed to be mycoplasma-negative using the LookOut mycoplasma PCR detection kit (Sigma-Aldrich) and were tested monthly.

Quantification of uptake by A431 cells

A total of 200,000 A431 cells in 12-well plates (CELLSTAR®, Greiner Bio-One GmbH) were cultivated for 24 h before exposure to NPs. After 24 h, media was replaced with NP dispersions (final concentration of 100 µg/mL), freshly prepared by diluting NP stocks in serum-free DMEM, or DMEM supplemented with different concentrations of fetal bovine serum (FBS). Following exposure to NPs for a time period of 24 h, cells were washed three times with PBS in order to ensure removal of loosely attached NPs from the cell membrane. To determine cell numbers, cells were harvested by trypsinization and counted using a CASY cell counter (Roche Diagnostics) according to the manufacturer's protocol. To measure the cellular iron content by ICP-MS, cells were lysed by adding 500 µL of 0.1% NaOH, dissolved by adding 100 µl of 65% HNO_3 and finally diluted to 2 mL with distilled H_2O prior to analysis. The iron content was expressed in pg Fe/cell. Cells without NP treatment served as controls for calculations.

***In vitro* assessment of nanotoxicity**

To assess cell viability following NP exposure, the A431 and HEK293 cells were seeded in 96-well plates at a density of 40,000 cells/0.1 mL/well and 60,000 cells/0.1 mL/well, respectively, and grown for 24 h prior to addition of NPs, which were freshly diluted to different final concentrations (0, 5, 10, 50, 100, 1000 µg/mL) in DMEM supplemented with 10% FBS. After 24 h incubation, the CellTiter 96® AQueous One

Solution Cell Proliferation Assay (Promega) as well as the CytoScan™ LDH Cytotoxicity Assay (G -Biosciences) were performed according to the manufacturer's instructions. For the latter assay, a triplicate set of wells was incubated with supplied lysis buffer to obtain maximum LDH release (positive control). NP-dependent LDH release was calculated relative to this value. In the proliferation assay, a triplicate set of wells containing untreated cells served as negative control. Cell viability upon NP exposure was expressed as a percentage relative to this negative control. All experiments were performed three times.

Acknowledgements

We thank Dr. Avinash Patel for support with protein-based techniques, Bezu Teschome for instrumental help with AFM, Stephan Weiss for support with zeta potential measurements, Utta Herzog for technical support during the cell culture work, and Karin Landrock for the elemental analyses. This work was supported by the Helmholtz Initiative and Networking Fund (Functional Nanomaterials for Multimodality Cancer Imaging (NanoTracking), project ID: VH-VI-421), the Australian Research Council through a Future Fellowship to B.G. (FT130100838) and a Discovery Outstanding Researcher Award and Discovery Grant to L.S. (DP130100816), and by an Alexander von Humboldt Foundation research fellowship to T.J.

Keywords: iron oxide nanoparticles • multimodal imaging • protein corona • proteomics • zwitterionic coatings

[1] K. Pombo-Garcia, K. Zarschler, L. Barbaro, J. A. Barreto, W. O'Malley, L. Spiccia, H. Stephan, B. Graham, *Small* **2014**, *10*, 2516-2529.
[2] K. Zarschler, L. Rocks, N. Licciardello, L. Boselli, E. Polo, K. P. Garcia, L. De Cola, H. Stephan, K. A. Dawson, *Nanomed. Nanotech. Biol. Med.* **2016**, *12*, 1663-1701.
[3] B. Pelaz, G. Charron, C. Pfeiffer, Y. Zhao, J. M. de la Fuente, X. J. Liang, W. J. Parak, P. Del Pino, *Small* **2013**, *9*, 1573-1584.
[4] C. D. Walkey, W. C. Chan, *Chem. Soc. Rev.* **2012**, *41*, 2780-2799.
[5] J. Feng, H. Liu, K. K. Bhakoo, L. Lu, Z. Chen, *Biomaterials* **2011**, *32*, 6558-6569.
[6] R. R. Arvizo, O. R. Miranda, D. F. Moyano, C. A. Walden, K. Giri, R. Bhattacharya, J. D. Robertson, V. M. Rotello, J. M. Reid, P. Mukherjee, *PLoS One* **2011**, *6*, e24374.
[7] S. T. Kim, K. Saha, C. Kim, V. M. Rotello, *Acc. Chem. Res.* **2013**, *46*, 681-691.
[8] D. F. Moyano, M. Goldsmith, D. J. Solfiell, D. Landesman-Milo, O. R. Miranda, D. Peer, V. M. Rotello, *J. Am. Chem. Soc.* **2012**, *134*, 3965-3967.
[9] A. Lesniak, F. Fenaroli, M. R. Monopoli, C. Aberg, K. A. Dawson, A. Salvati, *ACS Nano* **2012**, *6*, 5845-5857.
[10] A. Jedlovszky-Hajdú, F. B. Bombelli, M. P. Monopoli, E. Tombácz, K. A. Dawson, *Langmuir* **2012**, *28*, 14983-14991.
[11] D. F. Moyano, K. Saha, G. Prakash, B. Yan, H. Kong, M. Yazdani, V. M. Rotello, *ACS Nano* **2014**, *8*, 6748-6755.
[12] K. Saha, D. F. Moyano, V. M. Rotello, *Mater. Horiz.* **2014**, *1*, 102-105.
[13] C. C. Fleischer, U. Kumar, C. K. Payne, *Biomater Sci-Uk* **2013**, *1*, 975-982.
[14] C. C. Fleischer, C. K. Payne, *Acc. Chem. Res.* **2014**, *47*, 2651-2659.
[15] K. Pombo-García, S. Weiss, K. Zarschler, C.-S. Ang, R. Hübner, J. Pufe, S. Meister, J. Seidel, J. Pietzsch, L. Spiccia, H. Stephan, B. Graham, *ChemNanoMat* **2016**, *2*, 959-971.
[16] U. Sakulkhu, M. Mahmoudi, L. Maurizi, J. Salaklang, H. Hofmann, *Sci. Rep.* **2014**, *4*, 5020.
[17] Z. Estephan, P. Schlenoff, J. Schlenoff, *Langmuir* **2011**, *27*, 6794-6800.
[18] S. Mondini, M. Leonzino, C. Drago, A. M. Ferretti, S. Usseglio, D. Maggioni, P. Tornese, B. Chini, A. Ponti, *Langmuir* **2015**, *31*, 7381-7390.
[19] D. Kim, M. K. Chae, H. J. Joo, I. H. Jeong, J. H. Cho, C. Lee, *Langmuir* **2012**, *28*, 9634-9639.
[20] Z. Zhou, H. Liu, X. Chi, J. Chen, L. Wang, C. Sun, Z. Chen, J. Gao, *ACS Appl. Mater. Interfaces* **2015**, *7*, 28286-28293.
[21] W. Xiao, J. Lin, M. Li, Y. Ma, Y. Chen, C. Zhang, D. Li, H. Gu, *Contrast Media Mol. Imaging* **2012**, *7*, 320-327.
[22] M. P. Monopoli, D. Walczyk, A. Campbell, G. Elia, I. Lynch, F. B. Bombelli, K. A. Dawson, *J. Am. Chem. Soc.* **2011**, *133*, 2525-2534.
[23] Y. Yan, K. T. Gause, M. M. J. Kamphuis, C.-S. Ang, N. M. O'Brien-Simpson, J. C. Lenzo, E. C. Reynolds, E. C. Nice, F. Caruso, *ACS Nano* **2013**, *7*, 10960-10970.
[24] J. Liu, M. Yu, X. Ning, C. Zhou, S. Yang, J. Zheng, *Angew. Chem. Int. Ed.* **2013**, *52*, 12572-12576.
[25] D. E. Owens Iii, N. A. Peppas, *Int. J. Pharm.* **2006**, *307*, 93-102.
[26] K. Susumu, E. Oh, J. B. Delehanty, J. B. Blanco-Canosa, B. J. Johnson, V. Jain, W. J. t. Hervey, W. R. Algar, K. Boeneman, P. E. Dawson, I. L. Medintz, *J. Am. Chem. Soc.* **2011**, *133*, 9480-9496.
[27] Q. Dai, C. Walkey, W. C. W. Chan, *Angew. Chem. Int. Ed.* **2014**, *53*, 5093-5096.
[28] K. Knop, R. Hoogenboom, D. Fischer, U. S. Schubert, *Angew. Chem. Int. Ed.* **2010**, *49*, 6288-6308.
[29] J. S. Gebauer, M. Malissek, S. Simon, S. K. Knauer, M. Maskos, R. H. Stauber, W. Peukert, L. Treuel, *Langmuir* **2012**, *28*, 9673-9679.
[30] E. L. Foster, Z. Xue, C. M. Roach, E. S. Larsen, C. W. Bielawski, K. P. Johnston, *ACS Macro Letters* **2014**, *3*, 867-871.
[31] H. Wei, O. T. Bruns, O. Chen, M. G. Bawendi, *Integr. Biol.* **2013**, *5*, 108-114.
[32] K. Pombo-Garcia, K. Zarschler, J. A. Barreto, J. Hesse, L. Spiccia, B. Graham, H. Stephan, *RSC Adv.* **2013**, *3*, 22443-22454.
[33] D. Docter, U. Distler, W. Storck, J. Kuharev, D. Wunsch, A. Hahlbrock, S. K. Knauer, S. Tenzer, R. H. Stauber, *Nat. Protoc.* **2014**, *9*, 2030-2044.
[34] C. C. Fleischer, C. K. Payne, *J. Phys. Chem. B* **2014**, *118*, 14017-14026.
[35] W. Liu, J. Rose, S. Plantevin, M. Auffan, J. Y. Bottero, C. Vidaud, *Nanoscale* **2013**, *5*, 1658-1668.
[36] M. P. Monopoli, C. Aberg, A. Salvati, K. A. Dawson, *Nat. Nanotechnol.* **2012**, *7*, 779-786.
[37] S. Tenzer, D. Docter, J. Kuharev, A. Musyanovych, V. Fetz, R. Hecht, F. Schlenk, D. Fischer, K. Kiouptsi, C. Reinhardt, K. Landfester, H. Schild, M. Maskos, S. K. Knauer, R. H. Stauber, *Nat. Nanotechnol.* **2013**, *8*, 772-U1000.
[38] Z. Li, B. Tan, M. Allix, A. I. Cooper, M. J. Rosseinsky, *Small* **2008**, *4*, 231-239.
[39] Y. Chang, S. Chen, Q. Yu, Z. Zhang, M. Bernards, S. Jiang, *Biomacromolecules* **2007**, *8*, 122-127.
[40] R. Hu, G. Li, Y. Jiang, Y. Zhang, J. J. Zou, L. Wang, X. Zhang, *Langmuir* **2013**, *29*, 3773-3779.
[41] C. J. Huang, Y. Li, S. Jiang, *Anal. Chem.* **2012**, *84*, 3440-3445.
[42] Q. Dai, Y. Yan, C. S. Ang, K. Kempe, M. M. Kamphuis, S. J. Dodds, F. Caruso, *ACS Nano* **2015**, *9*, 2876-2885.
[43] P. J. Boersema, R. Raijmakers, S. Lemeer, S. Mohammed, A. J. R. Heck, *Nat. Protoc.* **2009**, *4*, 484-494.
[44] S. R. Saptarshi, A. Duschl, A. L. Lopata, *J Nanobiotechnology* **2013**, *11*, 26.
[45] J. Wang, U. B. Jensen, G. V. Jensen, S. Shipovskov, V. S. Balakrishnan, D. Otzen, J. S. Pedersen, F. Besenbacher, D. S. Sutherland, *Nano Lett.* **2011**, *11*, 4985-4991.

WILEY-VCH

[46] E. Dulkeith, M. Ringler, T. A. Klar, J. Feldmann, A. Munoz Javier, W. J. Parak, *Nano Lett.* **2005**, *5*, 585-589.
[47] R. B. Mujumdar, L. A. Ernst, S. R. Mujumdar, C. J. Lewis, A. S. Waggoner, *Bioconjug. Chem.* **1993**, *4*, 105-111.
[48] G. Kim, C. E. Yoo, M. Kim, H. J. Kang, D. Park, M. Lee, N. Huh, *Bioconjug. Chem.* **2012**, *23*, 2114-2120.
[49] G. R. Fulmer, A. J. M. Miller, N. H. Sherden, H. E. Gottlieb, A. Nudelman, B. M. Stoltz, J. E. Bercaw, K. I. Goldberg, *Organometallics* **2010**, *29*, 2176-2179.
[50] V. Nanjappa, J. K. Thomas, A. Marimuthu, B. Muthusamy, A. Radhakrishnan, R. Sharma, A. Ahmad Khan, L. Balakrishnan, N. A. Sahasrabuddhe, S. Kumar, B. N. Jhaveri, K. V. Sheth, R. Kumar Khatana, P. G. Shaw, S. M. Srikanth, P. P. Mathur, S. Shankar, D. Nagaraja, R. Christopher, S. Mathivanan, R. Raju, R. Sirdeshmukh, A. Chatterjee, R. J. Simpson, H. C. Harsha, A. Pandey, T. S. Prasad, *Nucleic Acids Res.* **2014**, *42*, D959-965.
[51] K. Zarschler, K. Prapainop, E. Mahon, L. Rocks, M. Bramini, P. M. Kelly, H. Stephan, K. A. Dawson, *Nanoscale* **2014**, *6*, 6046-6056.

WILEY-VCH

FULL PAPER

Activating Stealth Mode: Zwitterionic modification of polyacrylic acid-coated ultra-small super-paramagnetic iron oxide nanoparticles improves their ability to resist serum protein corona formation, with minimal cytotoxic effects on A431 and HEK293 cells. The availability of unreacted carboxylate groups enables attachment of additional moieties (fluorophore/radiochelate) for generating “stealth” multimodal imaging/theranostic probes.

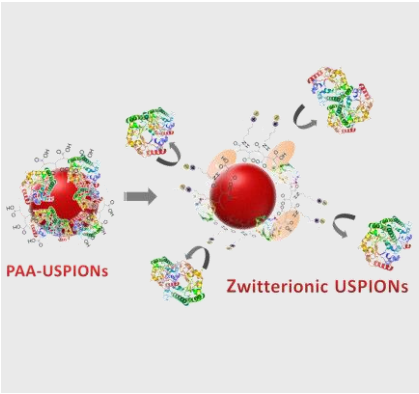

Karina Pombo-García, Carmen Rühl, Raymond Lam, José A. Barreto, Ching-Seng Ang, Peter J. Scammells, Peter Comba, Leone Spiccia, Bim Graham, Tanmaya Joshi,* and Holger Stephan**

Page No. – Page No.

Zwitterionic Modification of Ultra-Small Iron Oxide Nanoparticles for Reduced Protein Corona Formation

WILEY-VCH

Supporting information

Zwitterionic Modification of Ultra-Small Iron Oxide Nanoparticles for Reduced Protein Corona Formation

Karina Pombo-García,[a]^ Carmen Rühl,[b]^ Raymond Lam,[c] José A. Barreto,[d] Ching-Seng Ang,[d] Peter J. Scammells,[c] Peter Comba,[b] Leone Spiccia,[e] Bim Graham,*[c] Tanmaya Joshi,*[a] and Holger Stephan*[a]

[a] Dr. K. Pombo-Garcia, Dr. T. Joshi, Dr. H. Stephan
Institute of Radiopharmaceutical Cancer Research
Helmholtz-Zentrum Dresden-Rossendorf
D 01328 Dresden, Germany
Email: t.joshi@hzdr.de; h.stephan@hzdr.de

[b] MSc. C. Rühl, Prof. P. Comba
Heidelberg University,
Institute of Inorganic Chemistry and Interdisciplinary Centre for Scientific Computing
Im Neuenheimer Feld 270,
69120 Heidelberg, Germany

[c] R. Lam, Prof. P. J. Scammells, Assoc. Prof. B. Graham
Monash Insitute of Pharmaceutical Sciences
Monash University
Parkville, VIC 3052, Australia
Email: bim.graham@monash.edu

[d] Dr. J. A. Barreto, Prof. L. Spiccia
School of Chemistry
Monash University
Clayton, VIC 3800, Australia

[e] Dr. C.-S. Ang
BIO21 Molecular Science and Biotechnology Institute
The University of Melbourne
Melbourne, VIC 3010, Australia

[^] *These authors contributed equally to this work.*

Supporting information for this article is given via a link at the end of the document.

WILEY-VCH

Table S1. List of the proteins identified by mass spectrometry-dimethyl labeling of the proteins present in the corona of **ZW-L1** exposed to 80% HS at 37°C. Accession = Uniprot accession number, Average ratio PAA-USPIONs/**ZW-L1** = average amount of protein present in corona of PAA-USPIONs relative to that of **ZW-L1**, SD = Standard deviation, Quantifiable peptides = number of unique peptides matching to protein based on 1% false discovery and filter of ≥ 2 unique peptides per protein, MW [kDa] = molecular weight of protein, pI = isoelectric point of protein.

Accession	Description	Average ratio PAA-USPIONs/ **ZW-L1** Fold excess	MW [kDa]	pI	Quantificable peptides
NP_000005.2	alpha-2-macroglobulin precursor [Homo sapiens]	75.81	163.18	6.41	2
NP_000474.2	apolipoprotein C-II precursor [Homo sapiens]	54.64	11.27	4.71	2

WILEY-VCH

Table S2. List of the proteins identified by mass spectrometry-dimethyl labeling of the proteins present in the corona of **ZW-L2** exposed to 80% HS at 37°C. Accession = Uniprot accession number, Average ratio PAA-USPIONs/**ZW-L2** = average amount of protein present in corona of PAA-USPIONs relative to that of **ZW-L2**, SD = Standard deviation, Quantifiable peptides = number of unique peptides matching to protein based on 1% false discovery and filter of ≥ 2 unique peptides per protein, MW [kDa] = molecular weight of protein, pI = isoelectric point of protein.

Accession	Description	Average ratio PAA-USPIONs/ **ZW-L2** Fold excess	MW [kDa]	pI	Quantificable peptides
NP_000474.2	apolipoprotein C-II precursor [Homo sapiens]	24.825	11.3	7.05	3
NP_000030.1	apolipoprotein A-I preproprotein [Homo sapiens]	23.622	30.8	5.80	8
NP_001634.1	apolipoprotein A-II preproprotein [Homo sapiens]	12.132	11.2	6.40	2
NP_000473.2	apolipoprotein A-IV precursor [Homo sapiens]	10.338	45.3	6.28	2
NP_000468.1	serum albumin preproprotein [Homo sapiens]	2.974	69.3	6.62	7
NP_000055.2	complement C3 precursor [Homo sapiens]	2.202	187.0	5.38	5
NP_000031.1	apolipoprotein C-III precursor [Homo sapiens]	2.014	10.8	6.27	2
NP_001822.3	clusterin preproprotein [Homo sapiens]	0.595	52.5	5.76	5
NP_002611.1	platelet factor 4 variant precursor [Homo sapiens]	0.079	11.5	4.72	3

WILEY-VCH

Table S3. List of the proteins identified by mass spectrometry-dimethyl labeling of the proteins present in the corona of **ZW-L3** exposed to 80% HS at 37°C. Accession = Uniprot accession number, Average ratio PAA-USPIONs/**ZW-L3** = average amount of protein present in corona of PAA-USPIONs relative to that of **ZW-L3**, SD = Standard deviation, Quantifiable peptides = number of unique peptides matching to protein based on 1% false discovery and filter of ≥ 2 unique peptides per protein, MW [kDa] = molecular weight of protein, pI = isoelectric point of protein.

Accession	Description	Average ratio PAA-USPIONs/ **ZW-L3** Fold excess	MW [kDa]	pI	Quantificable peptides
NP_000375.2	apolipoprotein B-100 precursor [Homo sapiens]	46.837	515.2	4.72	13
NP_000629.3	vitronectin precursor [Homo sapiens]	10.625	54.3	5.76	4
NP_000055.2	complement C3 precursor [Homo sapiens]	2.152	187.0	6.62	11
NP_000468.1	serum albumin preproprotein [Homo sapiens]	1.486	69.3	5.38	7
NP_001634.1	apolipoprotein A-II preproprotein [Homo sapiens]	1.328	11.2	6.28	2
NP_000473.2	apolipoprotein A-IV precursor [Homo sapiens]	1.190	45.3	6.40	4
NP_001822.3	clusterin preproprotein [Homo sapiens]	1.184	52.5	5.41	4
NP_000030.1	apolipoprotein A-I preproprotein [Homo sapiens]	1.177	30.8	6.27	7
NP_000474.2	apolipoprotein C-II precursor [Homo sapiens]	0.958	11.3	9.10	3
NP_000031.1	apolipoprotein C-III precursor [Homo sapiens]	0.813	10.8	9.10	2

WILEY-VCH